RSC Advances

ROYAL SOCIETY OF CHEMISTRY

www.rsc.org/advances

RSC Advances

RSCPublishing

ARTICLE

Decomposition of S-nitroso Species

Cite this: DOI: 10.1039/xoxxoooooox

J. B. Dorado,[a] B. Z. Dlugogorski,[b*] E. M. Kennedy,[a] J. C. Mackie,[a] J. Gore,[c] M. Altarawneh[b]

Received ooth January 2015,
Accepted ooth January 2012

DOI: 10.1039/xoxxoooooox

www.rsc.org/

Nitrosation reactions and subsequent decomposition of S-nitroso ($RSNO^+$) species remain important in many biochemical processes as well as in industrial applications such as chemical gassing of emulsion explosives. This paper develops kinetic mechanisms of gas formation pathways in the decomposition of $RSNO^+$ species, particularly S-nitrosothioacetamide and S-nitrosothiourea, providing new kinetic and thermodynamic constants. At pH levels of 1 and below, decomposition proceeds exclusively via NO formation pathways. With decreasing acidity, molecular nitrogen formation emerges as an equally important product of S-nitrosothiourea, while NO remains the only product for S-nitrosothioacetamide. Theoretical calculations for reaction enthalpies further elucidate the gas formation pathways and proposed mechanisms, fitted to experimental data, afford kinetic rate constants. In both species, the S–N bonds split homolytically with activation energies of 70.9 and 118 kJ mol^{-1} for S-nitrosothioacetamide and S-nitrosothiourea, respectively. The electron donating effect of methyl substitution in S-nitrosothioacetamide engenders lower activation energies with the bimolecular reaction of $RSNO^+$ and RS occurring within the diffusion controlled regime at an activation energy of 17.6 kJ mol^{-1}. For S-nitrosothiourea, a further bimolecular reaction of two $RSNO^+$ molecules occurs irreversibly with an activation energy of 84.4 kJ mol^{-1}.

Introduction

Nitrosation reactions sparked interest in the biochemical field following the discovery of nitric oxide as a signalling molecule in many biological functions prompting research, for instance, in S-nitrosothiols as nitric oxide (NO) donors in vivo as well as in N-nitrosamines due to their carcinogenic properties.[1,2] However, diverse industrial functions extend to azo-dye production[3] and chemical gassing of emulsion explosives. In the latter, a substrate and a nitrosating agent react to generate nitrogen (N_2) gas bubbles in situ providing sensitisation of the emulsion to detonation. The decomposition of nitrosated compounds to either NO or N_2 often poses problems due to widely differing desirability of the two products. Therefore, it is important to determine the kinetics and mechanistic pathways of nitrosation in substrates that form N_2 and NO_x to optimise processes that are relevant to a particular application.

Nitrosation reactions in thiourea and thioacetamide are particularly interesting due to the inherent structural flexibility that allows intra- and inter-molecular transnitrosation. In these compounds, the initial nitrosation occurs at the sulfur atom due to its greater nucleophilicity and the subsequent NO^+ transfer to a deprotonated amine group results in rapid release of N_2. Previous studies proposed that nitrous acid initiated reactions with thiourea proceed via two pH-dependent pathways occurring in parallel. The first pathway results in the formation of thiocyanate and N_2 consequent of the S- to N-transnitrosation in S-nitrosothiourea, as studied earlier within the narrow range of pH 3.8−4.1. The second pathway forming disulfide and NO occurs at a lower pH but has not been studied in detail. For thioacetamide, nitrosation studies limit to the initial S-nitrosation, with largely unknown subsequent decomposition pathways.

Nitrosation potentially occurs at nitrogen or sulfur sites in aminothiols and aminothiones, but it is generally observed to occur at the sulfur atom producing S-nitroso species that exist in either *cis* or *trans* isomeric forms. The presence of *cis–trans* isomers signifies a transitional character between single and double S–N bonds.[4] Primary and secondary thionitrites favourably adopt *cis* conformation that is typically red in colour, while tertiary species preferentially exist as *trans* conformers that are green in colour due to steric reasons. Thionitrites display strong absorbance in the UV region (200–400 nm) and weaker transitions in the visible region (380–750 nm). Absorbance maxima of weaker transitions are found within the range 510–550 nm for red *n*-alkyl thionitrites and

550–605 nm for red-green *tert*-butyl thionitrites while dark red aromatic thionitrites are around 530 and 570 nm.[5-7] The reaction of nitrous acid with aminothiones thioacetamide and thiourea in acidic solutions results in yellow secondary S-nitroso adducts, allowing in situ studies that rely on UV spectroscopic properties reported in literature.[8]

S-nitroso compounds undergo different decomposition pathways depending on the conditions that are present. One such process represents the spontaneous thermal decomposition of RSNO observed in neutral aqueous solutions as in the two-stage reaction in Eqs. 1 and 2; where RS· denotes a thiyl radical. Photodecomposition occurs in thermally stable RSNOs in a similar manner. The stability of RSNO depends on both the strength of the S–N bond and the ease of S–S bridge formation.[9,10] Previous authors demonstrate that the homolytic splitting of the S–N bond is reversible[4,10] and the formation of the corresponding disulfide is the rate-limiting step. Applying calorimetric measurements, Lü et al. propose that, the homolytic S–N bond dissociation enthalpy [D_0(S–N)] is ~84 kJ mol^{-1} for aromatic RSNOs in comparison to 105 kJ mol^{-1} for aliphatic RSNOs.[11] Bartberger et al.[12] report a much higher values of 130–134 kJ mol^{-1} for primary to tertiary aliphatic S-nitrosothiols using the CBS-QB3 methodology,[13] with known accuracies of up to 8 kJ when compared to experimental data.

$$\mathrm{RSNO} \rightleftharpoons \mathrm{RS^{\cdot}} + \mathrm{NO} \quad (1)$$
$$\mathrm{RS^{\cdot}} + \mathrm{RS^{\cdot}} \rightarrow \mathrm{RSSR} \quad (2)$$

Experiments performed by Grossi and Montevechci[14] in refluxing solvents show that, thermal stability of RSNOs decreases with increasing bulkiness of the alkyl group. Although there is a clear indirect solvent effect on kinetic rates, tertiary nitrosothiols consistently decompose faster than primary nitrosothiols and this concurs with the conclusion by Martin-Diaconescu et al.[4] that S–N bonds in tertiary aliphatic S-nitrosothiols are weaker when compared to primary analogues. However, activation energies of 84–96 kJ mol^{-1} fall significantly lower than literature values[11,15] of 105 kJ for bond dissociation enthalpies of related aliphatic RSNOs. Under oxidative conditions, Zhao et al.[16] propose a nitrosonium catalysed cationic chain mechanism that explains the much faster S–N homolysis decomposition rate than expected. In aerated solutions, N_2O_3-mediated decomposition of RSNOs proceeds upon reaction of oxygen with nitric oxide. Such autocatalytic chain decomposition predominates over unimolecular S–N bond scission.[14]

For thiourea and substituted thioureas at higher acidities, the decomposition of the S-nitroso species consists of two parallel pathways represented by Eqs. 3 and 4. For S-nitrosothiourea, Eq. 3 translates to the formation of disulfide and nitric oxide radicals in Eq. 5, while Eq. 4 corresponds to a simple bimolecular reaction of two S-nitrosothiourea molecules in Eq. 6 producing nitric oxide radicals and the cationic disulfide, $(NH_2)_2CSSC(NH_2)_2{}^{2+}2X^-$, isolated by Werner in the form of the salt.[17,18]

$$\mathrm{RS} + \mathrm{RSNO^+} \rightarrow \mathrm{RSSR^{+\cdot}} + \mathrm{NO} \quad (3)$$
$$\mathrm{RSNO^+} + \mathrm{RSNO^+} \rightarrow \mathrm{RSSR^{2+}} + 2\mathrm{NO} \quad (4)$$
$$(\mathrm{NH_2})_2\mathrm{CS} + \mathrm{ONSC(NH_2)_2^+} \rightleftarrows (\mathrm{NH_2})_2\mathrm{CSSC(NH_2)_2^{+\cdot}} + \mathrm{NO} \quad (5)$$
$$2\mathrm{ONSC^+(NH_2)_2} \rightarrow 2\mathrm{NO} + (\mathrm{NH_2})_2\mathrm{CSSC(NH_2)_2^{2+}} \quad (6)$$

An *X*-ray study of Foss et al. confirms the structure of $(NH_2)_2C^+SSC^+(NH_2)_2$.[19] The kinetic stability of the cationic product CC'-dithiodiformamidinium ion investigated by García-Río et al.,[20] over a wide pH range of 1.9 to 9, suggests a decomposition mechanism via the reactive tautomer $(HN=)(NH_3^+)CSSC^+(NH_2)_2$ under base-catalysed conditions. In acidic solutions with pH of 0.3 to 1.8, this doubly charged cation reacts with nitrous acid as depicted in Eq. 7 at a slower rate than the $RSNO^+$ decomposition process.[21] Francisco et al. further studied the autocatalytic nitrosation of CC'-dithiodiformamidinium ion through thiocyanate ion arising from thiocyanogen hydrolysis.[22] The latter catalysis is not expected to occur where nitrous acid is the limiting reactant and at a pH of 1 and below.

$$6\mathrm{HNO_2} + 3(\mathrm{NH_2})_2\mathrm{CSSC}(\mathrm{NH_2})_2{}^{2+} \longrightarrow 6\mathrm{N_2} + 5\mathrm{HSCN} + \mathrm{H_2SO_4} + \mathrm{HCN} + 6\mathrm{H^+} + 8\mathrm{H_2O} \quad (7)$$

Subsequent intramolecular transnitrosation of S-nitrosothiourea occurs to form N_2 as depicted in Eq. 8, a pathway likely to dominate at higher pH.[23,24] Previous studies proposed direct N-nitrosation of thiourea, resulting in an unstable nitrosamine that decomposes to nitrogen.[25] The rate law did not follow first-order dependence on pH; this observation was explained by an initial step, which involved deprotonation of an amine site. However, this pathway was subsequently discounted as it required an unreasonably high pK_a of the amine site if the deprotonated thiourea reacted at an encounter rate of 15 000 M^{-1} s^{-1} typical for anionic nucleophiles at the same temperature.

$$\mathrm{ONSC(NH_2)_2^+} \rightarrow \mathrm{N_{2\,(g)}} + \mathrm{SCN^-} + \mathrm{H_2O} + 2\mathrm{H^+} \quad (8)$$

This study explores the decomposition of S-nitroso derivatives of thiourea and thioacetamide to gain a better understanding of gas formation pathways involved.

Materials and methods

Materials

The substrates deployed in experiments consist of >98.5 % thiourea (Riedel-de Haën) and >98 % thioacetamide (Sigma Aldrich) dissolved fresh prior to experiments. Nitrous acid served as the nitrosating agent, made by dissolving 99.5 % free flowing sodium nitrite (Sigma Aldrich) in solutions of excess perchloric acid. Perchloric acid was received at 70 % (Sigma Aldrich) and standardised by titration with sodium carbonate while 98 % anhydrous sodium perchlorate (Sigma Aldrich) was stored in a desiccator prior to use. Substrate concentrations varied between 10 and 60 mM with the nitrite kept at 2 mM for measurements covering a temperature range of 15–45 °C at 5 °C increments. Experimental conditions spanned a pH range of between 1 and 4 (0.5 pH increment) and ionic strength between 0.1 and 0.4 M (0.1 M increments). All solutions were prepared using distilled deionised water and reactant solutions were kept at the required ionic strength using sodium perchlorate.

Stopped-flow spectrophotometry

Applied Photophysics RX2000 stopped-flow mixing accessory, interfaced with Varian Cary50 spectrophotometer, allowed

kinetic studies for nitrosation reactions using a 1 cm path-length quartz cuvette. A Peltier temperature controller regulated the temperature in the mixing cell while a Grant water bath thermostatted the stopped-flow mixing circuit to ±0.1 °C. The dead time of the stopped-flow system was determined through the method of Matsumura et al.[26] using the second-order reaction of 2,6-dichloroindophenol (DCIP) with ascorbic acid originally proposed by Nakatani and Hiromi.[27]

Thioacetamide hydrolyses in acidic solutions, resulting in the formation of acetamide and hydrogen sulfide or thioacetic acid and ammonium ion.[28] Separate experiments performed by following the UV–vis spectra of thioacetamide and thiourea in acidic solutions revealed no significant interference of hydrolysis in the nitrosation measurements, which reach equilibrium in less than 300 ms. Spectroscopic properties determined previously guided absorbance selection to 420 nm for kinetics studies to avoid interference in signals as reported in previous studies.[23,29] In addition, trace quantities of copper ions in solution potentially inhibit proton addition at either the nitrogen or sulfur atom[28] and potentially act as catalysts in S-nitrosothiol decomposition.[30,31] Separate experiments (shown in Supplementary Information) ascertained negligible effect of EDTA addition on S-nitrosation and subsequent decomposition. An average of at least four data sets represented each of the six RS concentrations studied from 15 to 45 °C at intervals of 5 °C.

Gas-phase detection of products

The in-situ experiments depicted in Fig. 1 allow quantitative detection of N_2 and NO/NO_x by headspace sampling technique. Nitrosation reactions proceed in an aqueous solution within a 10 mL reactor and gaseous products are stripped from the reactor using high purity helium (99.999 %) as the mobile phase, flowing at 1.33 mL s^{-1}, allowing detection sensitivity up to 10 ppm for N_2. Chemiluminescence (Thermo 421HL NO_x analyser) facilitated the measurement of NO and NO_2 concentrations as low as 1 ppm, in the current study.[32] A 1000 ppm NO standard from Coregas Pty. Ltd. served to calibrate this analyser at the same flow rate as in experiments.

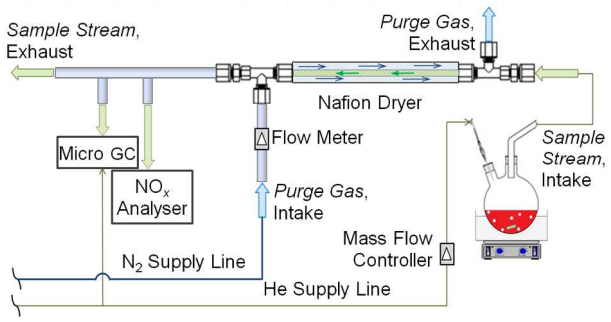

Fig. 1 Schematic of experimental setup for N_2/NO_x analysis.

For anaerobic experiments, gas chromatography through Varian CP4900 affords N_2 and Ar−O_2 measurements via Molsieve 5Å column and H_2O from PoraPLOT Q column with a thermal conductivity detector at column/injection temperatures of 80 °C. These measurements, taken at an interval of 2.25 min, monitor Ar–O_2, N_2, and H_2O at elution times of 0.91, 1.19, and 0.845 min, respectively, at a sample time of 30 s, run time of 80 s and stabilising time of 5 s. A system consisting of Nafion dryer installed in the sampling line removes moisture, while N_2 purge gas flows in counter-current direction at 4.7 mL s^{-1}. Zero chemiluminescence detection with NO calibration gas in the purge stream rules out cross contamination between purge and sample streams within the dryer. Flow checks at the exit of the Nafion dryer confirmed no leak within the sample stream. For experiments carried out in anaerobic conditions, sparging with carrier gas removes oxygen and leak tests guarantee a well-sealed system. At least three replicates establish gas formation trends at different pH.

Raman Analysis

Raman measurements were carried out using a Renishaw in*Via* system with a 785 nm diode laser coupled to an InPhotonics fibre optic sampling probe, which is connected to a sampling module, at around 6.7 mW laser power output. The Raman probe contains a coaxial two-fibre conduit wherein one fibre conveys the excitation signal and the other carries the captured photons. The scattered light is collected (180° backscattering geometry) along the same optical path as the incoming laser. Raman scattered light passes through a notch filter via a 1200 mm/groove grating that disperses the light over a CCD array detector.

Data Analysis

The Dynafit program[33] fits defined reaction mechanisms with the experimental data to determine the kinetic rate constants for S-nitrosation. The program uses the Levenberg–Marquardt algorithm for nonlinear least-squares regression to minimise the error between reaction progress curves and a solution of a system of first-order ordinary differential equations generated from the model reaction mechanisms. The Dynafit model incorporates reaction mechanisms with known rate constants quoted from literature. Adopting the same approach used by da Silva et al.[34] and Rayson et al.[35] for protonation equilibrium, the association rate constant of nitrous acid assumes a value of 10^{10} M^{-1} s^{-1}. Variation in initial estimates of kinetic rate constants verifies the convergence to a global minimum.

Gaussian Calculations

Considering ionic species in aqueous solutions, three solvation models calculate the free energy in the solution in conjunction with gas-phase free energies: conductor-like polarisable continuum model (CPCM) with united atom for Hartree–Fock (UAHF) definition for molecular cavity, equation formalism polarisable continuum model (IEFPCM) in conjunction with Bondi's definition for atomic radii, and solvation model using charge density (SMD). These models employ B3LYP functionals with 6-31+G(d,p) basis set and a further hybrid meta exchange-correlation functional M05-2X for SMD.

The free energy of solvation required calculations to be performed at the same level of theory and basis set size for both solvent and gas-phase models. Conformational variations with locally stable configurations determined in the gas-phase served as initial geometries for DFT optimisation in the aqueous phase. Moreover, geometry optimisation comprised both gas and aqueous phase calculations to account for any geometry relaxation upon solvation. The absence of imaginary frequencies confirmed the existence of true minima. All calculations involved the Gaussian 09 program.[36]

Results and discussion

Decomposition products

The decomposition of S-nitrosothioacetamide and S-nitrosothiourea proceed exclusively via NO_x formation pathways at pH 1 and below, with nitric oxide as the main product evident in Figs. 2 and 3. As the pH increases, different pathways emerge. The rate of gas formation consistently drops, due to dependence of initial nitrosation rate on the concentration of the active nitrosating agent derived from nitrous acid. Nitrous acid protonates to form nitrous acidium and equilibrates dinitrogen trioxide, which are both potential nitrosating agents. Very little gassing occurs at pH 4.6 where the dominant species is nitrite. S-nitrosothioacetamide decomposes at a faster rate, producing NO_x solely as the decomposition product with a conversion level of 100 ± 5 % on a total nitrite basis over the entire range of pH conditions studied. In the case of S-nitrosothiourea, NO_x yields drop to approximately 63 % at a pH of 2, concurrent with the detection of N_2 in the gas chromatographic analysis. There are two possible pathways for N_2 formation: direct nitrosation at an amine site or via S-nitrosation at the sulfur site and a subsequent transnitrosation to an amine site. Separate UV-vis experiments discussed in Supplementary Information show that the equilibrium mole fraction of S-nitrosothiourea exceeds 80 % at the same pH. Hence, it is likely that S to N transnitrosation plays a role in N_2 formation.

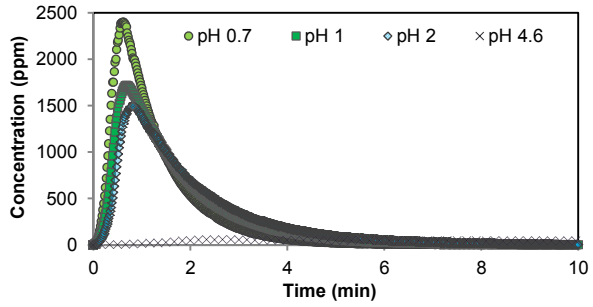

Fig. 2 Typical NO_x yields during decomposition of S-nitrosothioacetamide at varying pH, headspace sampling at 26 °C (n = 3, 1σ ≤ 3 %). $[TA]_0$ = 10 mM, $[NO_2^-]_0$ = 1 mM, and 1 M $NaClO_4$.

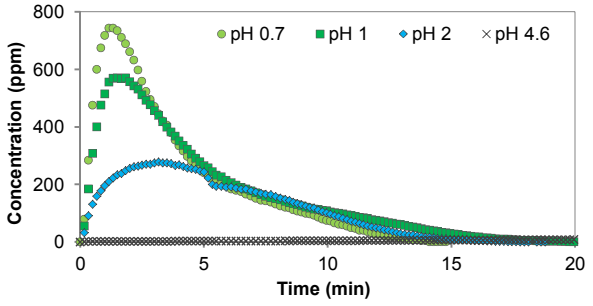

Fig. 3 Typical NO_x yields during decomposition of S-nitrosothiourea at varying acidity, headspace sampling at 26 °C (n = 3, 1σ ≤ 3 %). $[TA]_0$ = 10 mM, $[NO_2^-]_0$ = 1 mM, and 1 M $NaClO_4$.

While the disulfide products of S-nitrosothiourea have been elucidated previously,[8,21,23] very little is known in the case of S-nitrosothioacetamide. Concurrent with NO evolution, a pale yellow precipitate forms within the solution. It is of interest to investigate whether this constitutes a disulfide species, typical in S-nitroso species decomposition processes. Raman spectrometry represents a convenient technique to study disulfide bonds, as evident by the characteristic bands at 499 and 503 cm^{-1} in cystine[37-39] as well as with S–S stretching vibrational bands for some neurotoxins[40] and proteins[41]. Figure 4 shows three intense Raman characteristic bands of elemental sulfur replicated in the sample spectrum, conclusively disclosing the presence of an S-S bond moiety in the precipitate. Based on the ASTM Raman Shift Standard for Spectrometer Calibration,[42] the assigned band shifts are at 153.8, 219.1 and 473.2 cm^{-1}. Previous studies identify clusters of sulfur in the bacterial coat of a worm[43] (160, 225, and 480 cm^{-1}) as well mordenite single crystals containing sulfur[44] (160, 225, and 484 cm^{-1}). Hence, observed Raman shifts fall within reasonable range of these values. The Supplementary Information presents the UV–vis spectra of $RSNO^+$ species and explains consequent sulfur formation.

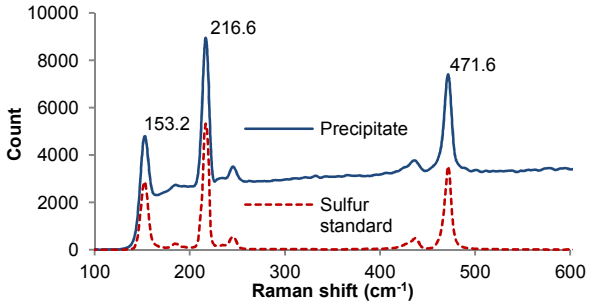

Fig. 4 Coincident Raman spectra of precipitate and sulfur calibration standard.

Kinetics of NO_x Formation Pathways

Identifying decomposition products assists in the study of mechanistic pathways and the kinetics involved in these reactions. Limiting the analysis to pH 1 and lower obviates further complications of parallel N_2 formation, allowing calculation of kinetic rates for NO_x formation. The decay curves of S-nitrosothioacetamide and S-nitrosothiourea in Fig. 5 exhibit different rate laws, with the former initially appearing as a linear zero-order plot. Hence, a bimolecular reaction of two S-nitrosothioacetamide molecules is unlikely.

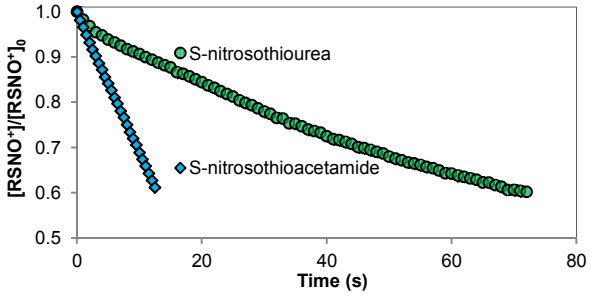

Fig. 5 $RSNO^+$ decay curves at 420 nm with $[RS]_{init}$ = 40 mM and $[NO_2^{-1}]_{init}$ = 2 mM at 1 M $NaClO_4$, pH 1 and 25 °C.

The rate of decomposition of S-nitrosothiourea decreases exponentially with time as expected with increase in concentration of products formed. Previous authors investigated the similar inhibiting effect of nitric oxide in the decomposition of nitrosyl thiocyanate[35] and S-nitrosothiourea.[45] For S-nitrosothioacetamide, the consequent sulfur formation results in

an interfering absorbance at the same wavelength. Hence, kinetic calculations restrict timeframes whereby decomposition progress does not exceed 20 % of initial $RSNO^+$ concentrations. In the kinetic studies, $[RS]_{init}$ and $[NO_2^-]_{init}$ represent the initial concentrations prior to S-nitrosation. The subscript "0" denotes the beginning of the $RSNO^+$ decay, where $t = 0$, $[RS]_0 = [RS]_{init} - [RSNO^+]_0$ and similarly for $[NO_2^-]_0$. The decay curve commences when S-nitrosation reaches equilibrium (i.e., $[RSNO^+]_{eq} = [RSNO^+]_0$).

Decomposition of S-nitrosothioacetamide

The decomposition pathway through homolytic scission of the S–N bond occurs independently of the nature of the nucleophilic substrate as depicted in Eq. 9, potentially explaining linear S-nitrosothioacetamide decay curves.

$$ONSCNH_2CH_3^+ \rightleftarrows SCNH_2CH_3^+\cdot + NO \quad (9)$$

However, first-order plots illustrate non-constant slopes with varying $[RSNO^+]_0$ concentrations; while first-order plots afford rate constants k_{obs} portraying direct proportionality with [RS]. Pseudo first-order plots based on Eq. 10 for which thioacetamide is in excess afford estimation of rate constants (discussed further in Supplementary Information). From such values, the intercepts of linear plots with thioacetamide concentrations are non-zero, which precludes Eq. 10 as the sole decomposition pathway. This indicates that at least two decomposition pathways are occurring in parallel, such as those described by Eqs. 1' and 3.

$$RSNO^+ \rightleftarrows RS^+\cdot + NO \quad (1')$$

$$SCNH_2CH_3 + ONSCNH_2CH_3^+ \xrightarrow{Nu} (CH_3NH_2)_2C_2S_2^+\cdot + NO \quad (10)$$

Further complications arise as a consequence of incomplete initial nitrosation of thioacetamide (Eq. 11), because of the equilibrium limitation (Fig. 6) as well as the parallel decomposition of nitrous acid according to the overall process presented in Eq. 12 involving N_2O_3 and N_2O_4 intermediates described by Eqs. 13 and 14.

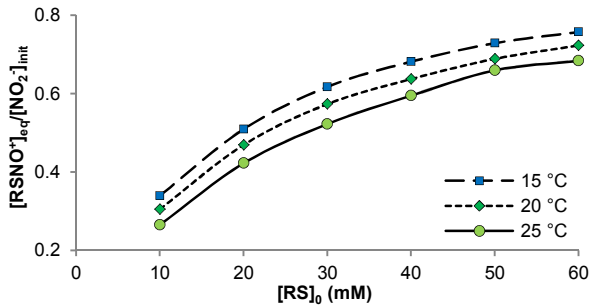

Fig. 6 Equilibrium mole fraction of $RSNO^+$ (S-nitrosothioacetamide) prior to decomposition ($n \geq 4$, $3\sigma \leq 1$ %). Experimental conditions are $[NO_2^-]_{init} = 0.002$ M, $[H^+] = 0.1$ M and $I = 1$ M, $NaClO_4$.

$$H^+ + HNO_2 + RS \rightleftarrows RSNO^+ + H_2O \quad (11)$$

$$3HNO_2 \rightleftarrows 2NO + NO_3^- + H^+ + H_2O \quad (12)$$

$$2HNO_2 \rightleftarrows NO + NO_2 + H_2O \quad (13)$$

$$2HNO_2 \rightleftarrows N_2O_3 + H_2O \quad (13a)$$

$$N_2O_3 \rightleftarrows NO + NO_2 \quad (13b)$$

$$2NO_2 + H_2O \rightleftarrows HNO_2 + NO_3^- + H^+ \quad (14)$$

$$NO_2 + NO_2 \rightleftarrows N_2O_4 \quad (14a)$$

$$N_2O_4 + H_2O \rightleftarrows HNO_2 + NO_3^- + H^+ \quad (14b)$$

Schwarz and White[46] provide values of rate constants for Eqs. 13 and 14. To account for the effect of temperature, Schwartz and White referenced theoretical results from a previous investigation[47] for enthalpies of reaction and activation energies. The Supplementary Information tabulates the relevant values. Several Dynafit models are used to evaluate different reaction mechanisms, considering the influence of S-nitrosation and nitrous acid decomposition reactions as well as the reversibility of Eqs. 1 and 3. For the cationic nitroso species, Eq. 1 is thus equivalently transformed as Eq. 1'. Inclusion of the nitrous acid decomposition pathway did not result in consistent rate constant trends with temperature. This is likely due to errors compounded by the exponential relation of theoretically obtained enthalpies of reaction with equilibrium constants, which were used to determine kinetic rates of reverse reactions. The mechanism outlined in Table 1, consisting of a bimolecular reaction and a reversible unimolecular decomposition pathway, delivers the best fit with data. Figure 7 depicts typical reaction progress curves fitted with this mechanism at 25 °C, while Fig. 8 illustrates increased rates with temperature.

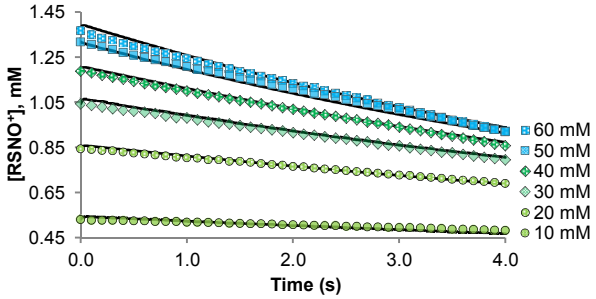

Fig. 7 Overlap of experimental data and kinetic model for S-nitrosothiacetamide decomposition. ($[H^+] = 0.1$ M, $[NO_2^-]_{init} = 0.002$ M, $I = 1$ M, $NaClO_4$ and 25 °C; $n \geq 4$, $3\sigma \leq 1$ %).

Table 1 Reaction mechanisms for S-nitrosothioacetamide decomposition

Eq. No.	$k_{f,25\,°C}$	E_a (kJ mol^{-1})
11*	15 800 M^{-1} s^{-1}	54.9
3	0.475 M^{-1} s^{-1}	17.6
1'	0.120 s^{-1}	70.9

*Covered in a separate study, experimental values.

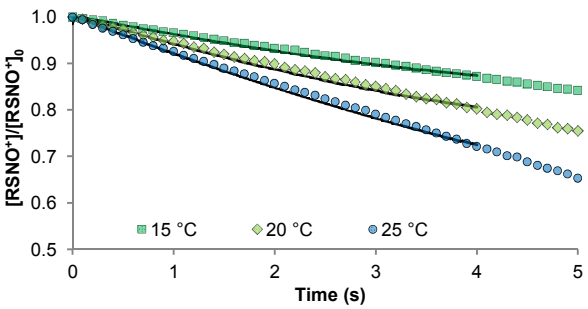

Fig. 8 Typical S-nitrosothioacetamide decay curves showing increased kinetic rates with temperature ($[RS]_{init} = 40$ mM and $[NO_0^{-1}]_{init} = 2$ mM at 1 M $NaClO_4$ and pH 1; $n \geq 4$, $1\sigma \leq 1$ %).

This current work reveals the decomposition kinetics of S-nitrosothioacetamide for the first time. The kinetic rate constant of 0.475 M^{-1} s^{-1}, for the bimolecular reaction between a free thioacetamide and S-nitrosothioacetamide (Eq. 3) at 25 °C, resemble that of nitrosothiourea. For nitrosothioacetamide, the activation energy falls lower at 17.6 kJ mol^{-1}, occurring in the diffusion controlled regime. This low activation energy predicates on the electron donating effect of methyl substitution for one of the two amine groups of thiourea. The solvated $RSSR^{+}\cdot$ structure rapidly decomposes to form sulfur precipitate.

The activation energy obtained for homolytic splitting of the S–N bond falls below the expected bond dissociation energies for neutral aliphatic S-nitroso structures. It would appear that cationic S-nitroso species are less stable than neutral species, consistent with longer S–N bonds predicted theoretically. The cationic structures in both gas and aqueous phase calculations exhibit elongated S–N bond lengths of around 2.1 Å that are indicative of very weak bonds. These S–N bond lengths exceed the 1.7–1.9 Å computed theoretically for neutral S-nitroso species like HSNO and methyl thionitrite or the values obtained from crystallographic data for a group of organic thionitrites.[48,49]

Decomposition of S-nitrosothiourea

The mechanism proposed in literature (Mechanism 2, Table 2) yielded excellent model–data conformity as can be seen in Fig. 9, with activation energies for Eqs. 3 and 4 differing by around 4.8 kJ based on Arrhenius plots in the Supplementary Information. This model consists of first-order and second order terms in $RSNO^{+}$. Despite the excellent fit of this mechanism with the data, the equilibrium concentrations of $RSNO^{+}$ defining the onset of decomposition kinetics do not approach full conversion of initial nitrite concentration as shown in Fig. 10. This incomplete conversion compels the integration of an initial S-nitrosation step in the overall mechanism. Furthermore, separate experiments confirm that pH does not affect the decomposition process at high acidities (in Supplementary Information).

Table 2 Reaction mechanisms[21,45] proposed in literature for formation of NO from nitrosothiourea and enthalpies from theoretical calculations

Eq. No.	$k_{f,25\,°C}$ (M^{-1} s^{-1})	ΔH_T (kJ)	E_a (kJ mol^{-1})
3	0.70	33.8	51.7
4	3.4	26.1	46.9

*Average values taken from different solvation models

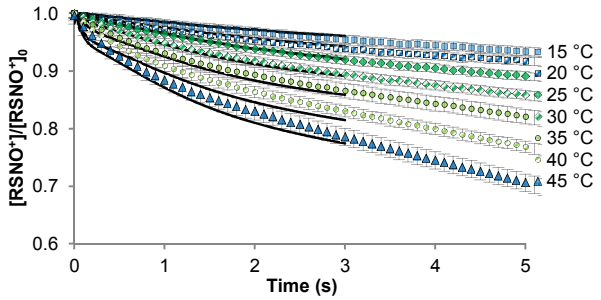

Fig. 9 Overlap of experimental data and kinetic model (Mechanism 2) for S-nitrosothiourea decomposition at varying temperature ($n \geq 4$, 3σ shown). Experiment conditions at $[H^+]$ = 0.1 M, $[NO_2^-]_{init}$ = 0.002 M, $[RS]_{init}$ = 0.04 M, and I = 1 M, $NaClO_4$.

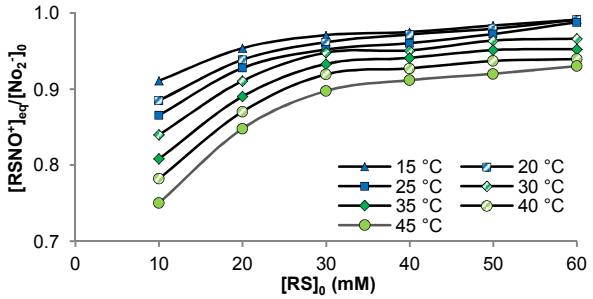

Fig. 10 Equilibrium mole fraction of $RSNO^{+}$ (S-nitrosothiourea) prior to decomposition. Experiment conditions are $[NO_2^-]_{init}$ = 0.002 M, $[H^+]$ = 0.1 M and I = 1 M, $NaClO_4$ ($n \geq 4$, $3\sigma < 1.5$ %)

For cationic S-nitroso species, a typically elongated S–N bond weakly links the NO molecule, explaining the susceptibility to unimolecular decomposition via homolytic splitting (Eq. 1'). The decomposition trend displays a clear first order dependence on thiourea concentration, which further lends credence to Eq. 3 proceeding as the electronically dense sulfur in free thiourea facilitates the release of the NO leaving group by forming an S–S bond with the electron deficient sulfur in the cationic radical. Moreover, the inhibitory effect of NO only applies to the first order term in $RSNO^{+}$ (as in Eq. 3),[21,45] plausibly the case, due to the unlikely nature of a reverse termolecular reaction between two NO radicals and the dicationic disulfide.

The bimolecular reaction of two S-nitrosothiourea species produces the symmetrical disulfide group and two NO molecules in an unusual elementary reaction. Previous studies[21,45] including metal-ion-catalysed dark decomposition of S-nitrosothiols[50] report a similar rate dependency. However, a true second order rate dependence was not observed. On the other hand, HNO_2 catalysis clearly develops where nitrous acid is in excess and quantitative conversion to S-nitrosothiourea occurs rapidly with no notable interference to decomposition.[21] Eq. 7 likely contributes to this effect and complicates the observed kinetics, compounded further by thiocyanogen hydrolysis that forms thiocyanate ions. Excess nitrous acid nitrosates the latter by-product to nitrosyl thiocyanate, which then absorbs significantly at the wavelength followed (i.e., 420 nm). Hence, kinetic analyses are limited to conditions where thiourea is in excess.

A theoretical approach explores the decomposition pathways further, particularly the elementary reactions involved in the bimolecular process of two $RSNO^{+}$ molecules. Table 3 lists alternative pathways to that of Eq. 4, as a multi-step mechanism, employing different solvation models. Based on the SM1 model, the unimolecular decomposition of $RSNO^{+}$ via homolytic S–N bond cleavage to form $RS^{+}\cdot$ and NO occurs at a reaction enthalpy of 113 kJ for S-nitrosothiourea. On the other hand, the unsymmetrical $RSSR^{+}\cdot$ exhibits a very weak S–S bond indicative of a charged dipole interaction of an RS and an $RS^{+}\cdot$ species. A unimolecular radical cation breakdown to RS and $RS^{+}\cdot$ proceeds at a reaction enthalpy of 81 kJ. While the reverse reaction is favourably exothermic, a similarly exothermic pathway involves a reaction between $RS^{+}\cdot$ and $RSNO^{+}$ to form $RSSR^{2+}$. Hence, if $RSSR^{2+}$ formation proceeds via Eq. 16, it is likely that unimolecular radical cation breakdown contributes to the evolution of $RS^{+}\cdot$ as this is a less energetic pathway. Although disulfide bridging of two cationic radicals in Eq. 17 is even more exothermic at -193 kJ, a

bimolecular reaction, of two molecules of a species that exists at very low concentrations, renders this pathway highly improbable.

$$RSSR^{+}\cdot \rightleftarrows RS^{+}\cdot + RS \quad (15)$$
$$RSNO^{+} + RS^{+}\cdot \rightleftarrows RSSR^{2+} + NO \quad (16)$$
$$RS^{+}\cdot + RS^{+}\cdot \rightleftarrows RSSR^{2+} \quad (17)$$

Table 3 Enthalpy change of reaction for alternate reaction steps considered in the decomposition of S-nitrosothiourea.

Eq. No.	$\Delta_r H$ (kJ)			
	SM1	SM2	SM3	SM4
1'	112.8	111.1	96.7	108.2
15	81.1	72.6	87.9	72.6
16	-80.2	-91.0	-119.2	-82.8
17	-192.9	-202.0	-215.9	-191.0

SM1: IEFPCM/UFF, UB3LYP/6-311G(d,p); SM2: B3LYP/6-311+G(d,p) CPCM (UAHF); SM3: M052X/6-311+G(d,p) SMD; SM4: B3LYP/6-311+G(d,p) SMD

Collings et al. found that the kinetic rate constant for Eq. 3 decreased by 65 % in NO-saturated solutions while Eq. 4 remained unaffected.[45] The fact that NO inhibition affects the first-order term in $RSNO^{+}$ conveys significance of a back reaction for Eq. 3. This reduces the likelihood of $RS^{+}\cdot$ formation, via unimolecular breakdown of the $RSSR^{+}\cdot$ product, as the contributing pathway for production of $RSSR^{2+}$. Moreover, the net reaction comprising Eqs. 3 and 15 suggests that the kinetic rates involved are unaffected by an increase in RS concentration. In contrast, experimental data display a stark increase in kinetic rate with an increase in RS concentration.

Combinations of these parallel reactions form part of a series of potential mechanisms. Mechanism 3, shown in Table 4 displayed the most exactness with respect to experimental data, and whereby activation energies fall within the expected range of values in literature (Arrhenius plots in Supplementary Information). In particular, Eq. 3 at 60.5 kJ displays excellent agreement with 60.9 kJ published by Garley and Stedman.[21] Homolytic scission of the S–N bond concurs with the projected bond dissociation enthalpy of 105–134 kJ for aliphatic S-nitrosothiol structures.[11,12] An activation energy of 84.4 kJ for the bimolecular reaction of two $RSNO^{+}$ molecules in Eq. 4 posted a larger difference, exceeding the published value of 50.8 kJ.[21] Solvation leads to a net decrease in the enthalpy and entropy of formation of an ion. The more solvated doubly charged ion in transition state, compared to two singly charged species in the initial state, contributes to the lower activation energy involved in $RSNO^{+}$ bimolecular reaction compared to S–N bond cleavage. Minor differences in reaction conditions, such as ionic strength, could cause differences in activation energies measured. The higher value obtained in the present study for Eq. 17 is more coherent with an energy intensive reaction comprising two cationic species and the concerted scission of two S–N bonds resulting in two free NO molecules and a stable CC'-dithiodiformamidinium ion. Furthermore, the forward kinetic rate constants of 0.56 and 5.00 M^{-1} s^{-1} for Eqs. 3 and 4 at 25 °C are very close to 0.59 and 5.25 M^{-1} s^{-1} published previously.[45] Nonetheless, a nonelementary reaction comprising two or more reaction steps remains possible.

Table 4 Reaction mechanism for S-nitrosothiourea decomposition (Mechanism 3)

Eq. No.	$k_{f,25\,°C}$	ΔH_T ** (kJ)	E_a (kJ mol^{-1})
11*	24 000 M^{-2} s^{-1}	-29.6	66.1
1'	0.014 s^{-1}	110	118
3	0.56 M^{-1} s^{-1}	33.8	60.5
4	5.00 M^{-1} s^{-1}	26.1	84.4

*From a separate study, experimental values. **Average values from different solvation models (in Supplementary Information) for Eqs. 1', 3 and 4.

Figure 11 illustrates the mechanistic fit of the model to experimental data at different temperatures. In fitting the proposed mechanism, we have ensured that the drop in $RSNO^{+}$ concentration at equilibration time, which constitutes the start of experimental data, does not exceed the experimental error. Despite this, some departure between experimental data and the model persists due to errors associated with the rate constants of initial S-nitrosation. However, the model follows the experimental measurements to within ±5 %. The presence of NO inhibits the initial rapid decomposition as observed previously,[45] mainly due to the reversibility of Eq. 3. At longer timeframes, the concentration–time plots in Fig. 12 display identical slopes. This is possibly due to other effects that are unaffected by NO, as in the case of S-nitrosothiocyanate decomposition.[35] The influence of mass transfer intensifies as nucleation initiates NO bubble formation subsequently enhancing desorption.[51] Furthermore, saturation of NO occurs faster than expected to arise at complete decomposition of $RSNO^{+}$ at 25 °C.[52] This is because, for a non-ionic species dissolved in a solution of electrolyte, its solubility decreases and bubbles commence to form at lower concentrations of dissolved gas. This coincides with observed bubble formation at earlier stages of decomposition, whereby elevated temperatures hastens the process due to the reduction in solubility and increased diffusivity.[53,54]

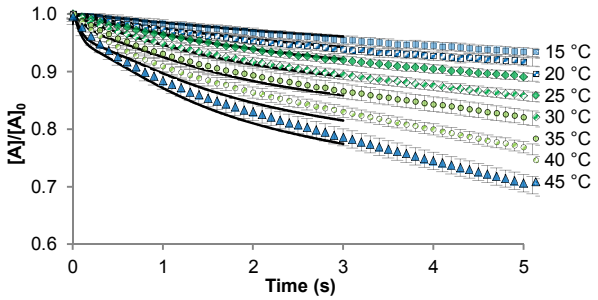

Fig. 11 Overlap of experimental data and kinetic model (Mechanism 3) for S-nitrosothiourea decomposition at varying temperature ($[H^{+}]$ = 0.1 M, $[NO_2^{-}]_{init}$ = 0.002 M, $[RS]_{init}$ = 0.04 M, I = 1 M, NaClO4; $n \geq 4$, 3σ shown).

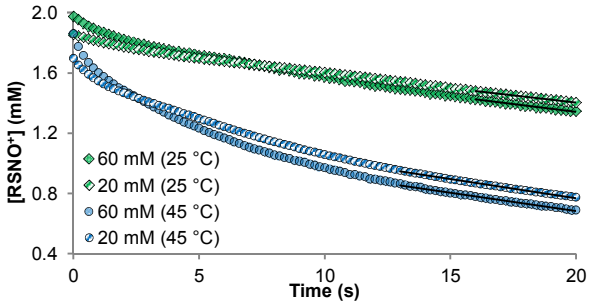

Fig. 12 Concentration-time plots of S-nitrosothiourea decomposition ($[H^{+}]$ = 0.1 M $HClO_4$, I = 1 M, $NaClO_4$).

Conclusions

This paper presents the first quantified evidence for gas formation pathways in the decomposition of S-nitroso adducts of thioacetamide and thiourea. Under conditions where the pH is 1 or below, decomposition proceeds exclusively through NO_x formation pathways. Previous studies depict a decomposition rate law consisting of two terms representing bimolecular reactions of $RSNO^+$ with a free RS species and another $RSNO^+$ molecule. Based on the reaction enthalpies, theoretical calculations elucidate the gas formation pathways involved. We present new mechanisms describing a more comprehensive model accounting for incomplete conversion to $RSNO^+$ species during initial S-nitrosation, which were fitted to kinetic data to determine rate constants. Both S-nitroso species split homolytically with activation energies of 70.9 and 118 kJ for S-nitrosothioacetamide and S-nitrosothiourea, respectively. The activation energies involved in $RSNO^+$ species fall lower than the bond dissociation energies of neutral S-nitroso compounds in concurrence with longer S–N bonds obtained theoretically for $RSNO^+$ species. The electron donating effect of methyl substitution in S-nitrosothioacetamide facilitates lower activation energies, and the bimolecular reaction of $RSNO^+$ and RS occurs within the diffusion controlled regime at an activation energy of 17.6 kJ. For S-nitrosothiourea, a further bimolecular reaction of two $RSNO^+$ molecules occurs irreversibly at an activation energy of 84.4 kJ mol^{-1}. This is expectedly higher than the 60.5 kJ mol^{-1} activation in the RS and $RSNO^+$ reaction as it involves two cationic species and a concerted scission of two S–N bonds resulting in two NO molecules and a stable CC'-dithiodiformamidinium ion.

Acknowledgements

This study was funded by the Australian Research Council and Dyno Nobel Asia Pacific, with support of computational resources from the National Computational Infrastructure (NCI).

Notes and references

[a] Process Safety and Environment Protection Research Group, School of Engineering, The University of Newcastle, Callaghan, NSW 2308, Australia

[b] School of Engineering and Information Technology, Murdoch University, 90 South Street, Murdoch WA 6150, Australia. Email: B.Dlugogorski@murdoch.edu.au

[c] Dyno Nobel Asia Pacific Pty. Ltd., Mt Thorley Technical Centre 5 Woodlands Road, Mt. Thorley NSW 2330, Australia

Electronic Supplementary Information (ESI) available: [S-Nitrosothioacetamide decomposition (reaction mechanism, Arrhenius and data–model concentration–time plots, rate constants of S-nitrosation and HNO_2 decomposition, formation of sulfur, decomposition kinetics), S-nitrosothiourea decomposition (reaction mechanisms, effect of EDTA addition), thiourea and thioacetamide nitrosation at pH 2, further comments to gas-phase detection of products, theoretical calculations, miscellaneous figures]. See DOI: 10.1039/b000000x/

1 Tricker, A. R.; Preussmann, R. *Mutation Research/Genetic Toxicology* **1991**, *259*, 277.
2 Lijinsky, W. *Cancer and Metastasis Reviews* **1987**, *6*, 301.
3 Hart, H. *Organic Chemistry: A Short Course*; 8th ed.; Houghton Mifflin Co.: Boston, 1991.
4 Martin-Diaconescu, V.; Perepichka, I.; Bohle, D. S.; Kennepohl, P. *Canadian Journal of Chemistry* **2011**, *89*, 93.
5 Oae, S.; Kim, Y. H.; Fukushima, D.; Shinhama, K. *Journal of the Chemical Society, Perkin Transactions 1* **1978**, 913.
6 Stamler, J. S.; Toone, E. J. *Current Opinion in Chemical Biology* **2002**, *6*, 779.
7 Barrett, J.; Debenham, D. F.; Glauser, J. *Chemical Communications* **1965**, 248.
8 Collings, P.; Al-Mallah, K.; Stedman, G. *Journal of the Chemical Society, Perkin Transactions 2* **1975**, 1734.
9 Szaciłowski, K.; Stasicka, Z. *Progress in Reaction Kinetics and Mechanism* **2001**, *26*, 1.
10 Bainbrigge, N.; Butler, A. R.; Görbitz, C. *Journal of the Chemical Society, Perkin Transactions 2* **1997**, 351.
11 Lü, J.-M.; Wittbrodt, J. M.; Wang, K.; Wen, Z.; Schlegel, H. B.; Wang, P. G.; Cheng, J.-P. *Journal of the American Chemical Society* **2001**, *123*, 2903.
12 Bartberger, M. D.; Mannion, J. D.; Powell, S. C.; Stamler, J. S.; Houk, K. N.; Toone, E. J. *Journal of the American Chemical Society* **2001**, *123*, 8868.
13 Levy, J. B. *Journal of the American Chemical Society* **1956**, *78*, 1780.
14 Grossi, L.; Montevecchi, P. C. *Chemistry – A European Journal* **2002**, *8*, 380.
15 Benson, S. W. *Chemical Reviews* **1978**, *78*, 23.
16 Zhao, Y.-L.; McCarren, P. R.; Houk, K. N.; Choi, B. Y.; Toone, E. J. *Journal of the American Chemical Society* **2005**, *127*, 10917.
17 Werner, E. A. *Journal of Chemical Society Chemical Communications* **1912**, *101*, 2180.
18 Werner, E. A. *Journal of the Chemical Society, Transactions* **1912**, *101*, 2166.
19 Foss, O.; Johnsen, J.; Tvedten, O. *Acta Chemica Scandinavia* **1958**, *12*, 1782.
20 García-Río, L.; Munkley, C. G.; Stedman, G. *Journal of the Chemical Society, Perkin Transactions 2* **1996**, 159.
21 Garley, M. S.; Stedman, G.; Miller, H. *Journal of the Chemical Society, Dalton Transactions* **1984**, 1959.
22 Francisco, V.; García-Río, L.; Antonio Moreira, J.; Stedman, G. *New Journal of Chemistry* **2008**, *32*, 2292.
23 Al-Mallah, K.; Collings, P.; Stedman, G. *Journal of the Chemical Society, Dalton Transactions* **1974**, 2469.
24 da Silva, G.; Dlugogorski, B. Z.; Kennedy, E. M. *AIChE Journal* **2006**, *52*, 1558.
25 da Silva, G.; Dlugogorski, B. Z.; Kennedy, E. M. *Chemical Engineering Science* **2006**, *61*, 3186.
26 Matsumura, K.; Enoki, Y.; Kohzuki, H.; Sakata, S. *Japanese Journal of Physiology* **1990**, *40*, 567.
27 Nakatani, H.; Hiromi, K. *Journal of Biochemistry* **1980**, *87*, 1805.
28 Rosenthal, D.; Taylor, T. I. *Journal of the American Chemical Society* **1960**, *82*, 4169.

29 Collings, P.; Al-Mallah, K.; Stedman, G. *Journal of Chemical Society Perkin II* **1975**, 1734.
30 Toubin, C.; Yeung, D. Y. H.; English, A. M.; Peslherbe, G. H. *Journal of the American Chemical Society* **2002**, *124*, 14816.
31 He, Y.; Sanders, W. A.; Lin, M. C. *Journal of Physical Chemistry A* **1988**, *92*, 5474.
32 Coneski, P. N.; Schoenfisch, M. H. *Chemical Society Reviews* **2012**, *41*, 3753.
33 Kuzmič, P. *Analytical Biochemistry* **1996**, *237*, 260.
34 da Silva, G.; Dlugogorski, B. Z.; Kennedy, E. M. *International Journal of Chemical Kinetics* **2007**, *39*, 645.
35 Rayson, M. S.; Mackie, J. C.; Kennedy, E. M.; Dlugogorski, B. Z. *Inorganic Chemistry* **2011**, *50*, 7440.
36 Frisch, M. J.; Trucks, G. W.; Schlegel, H. B.; Scuseria, G. E.; Robb, M. A.; Cheeseman, J. R.; Scalmani, G.; Barone, V.; Mennucci, B.; Petersson, G. A.; Nakatsuji, H.; Caricato, M.; Li, X.; Hratchian, H. P.; Izmaylov, A. F.; Bloino, J.; Zheng, G.; Sonnenberg, J. L.; Hada, M.; Ehara, M.; Toyota, K.; Fukuda, R.; Hasegawa, J.; Ishida, M.; Nakajima, T.; Honda, Y.; Kitao, O.; Nakai, H.; Vreven, T.; Montgomery, J. A.; Peralta, J. E.; Ogliaro, F.; Bearpark, M.; Heyd, J. J.; Brothers, E.; Kudin, K. N.; Staroverov, V. N.; Kobayashi, R.; Normand, J.; Raghavachari, K.; Rendell, A.; Burant, J. C.; Iyengar, S. S.; Tomasi, J.; Cossi, M.; Rega, N.; Millam, J. M.; Klene, M.; Knox, J. E.; Cross, J. B.; Bakken, V.; Adamo, C.; Jaramillo, J.; Gomperts, R.; Stratmann, R. E.; Yazyev, O.; Austin, A. J.; Cammi, R.; Pomelli, C.; Ochterski, J. W.; Martin, R. L.; Morokuma, K.; Zakrzewski, V. G.; Voth, G. A.; Salvador, P.; Dannenberg, J. J.; Dapprich, S.; Daniels, A. D.; Farkas; Foresman, J. B.; Ortiz, J. V.; Cioslowski, J.; Fox, D. J.; Revision B.01 ed. Wallingford CT, 2009, p Gaussian 09 Software.
37 Johnson, C. R.; Asher, S. A. *Journal of Raman Spectroscopy* **1987**, *18*, 345.
38 Ikeguchi, M.; Shimizu, S.; Nakamura, S.; Shimizu, K. *Journal of Physical Chemistry B* **1998**, *102*, 5891.
39 Van Wart, H. E.; Lewis, A.; Scheraga, H. A.; Saeva, F. D. *Proceedings of the National Academy of Sciences* **1973**, *70*, 2619.
40 Tu, A. T. *Journal of the Chinese Chemical Society* **2003**, *50*, 10.
41 Li, T.; Yamane, H.; Arakawa, T.; Narhi, L. O.; Philo, J. *Protein Engineering* **2002**, *15*, 59.
42 American Society for Testing and Materials international: West Conshohocken, 2007.
43 Himmel, D.; Maurin, L. C.; Gros, O.; Mansot, J.-L. *Biology of the Cell* **2009**, *101*, 43.
44 Poborchii, V. V. *Chemical Physical Letters* **1996**, *92*, 230.
45 Collings, P.; Garley, M.; Stedman, G. *Journal of the Chemical Society, Dalton Transactions* **1981**, 331.
46 Schwartz, S. E.; White, W. H. *Advances in Environmental Science and Technology* **1983**, *12*, 1.
47 Rayson, M. S.; Mackie, J. C.; Kennedy, E. M.; Dlugogorski, B. Z. *Inorganic Chemistry* **2012**, *51*, 2178.
48 Timerghazin, Q. K.; Peslherbe, G. H.; English, A. M. *Physical Chemistry Chemical Physics* **2008**, *10*, 1532.
49 Ruano, C.; Otero, J. C.; Arenas, J. F.; Soto, J. *Chemical Physics Letters* **2012**, *553*, 17.
50 Ignarro, L. J. *Nitric Oxide Pathology and Pathobiology*; Academic Press: San Diego, 2000.
51 Marta, F.; Seres, L. *Berichte der Bunsengesellschaft für physikalische Chemie* **1966**, *70*, 921.
52 Gislason, J.; Wharry, S. M. *Journal of Chromatographic Science* **2000**, *38*, 129.
53 Berski, S.; Latajka, Z.; Gordon, A. J. *Chemical Physics Letters* **2010**, *493*, 392.
54 Coulson, C. B.; Davies, R. I.; Luna, C. *Analyst* **1960**, *85*, 203.